Solar wind origin in coronal funnels and correlation heights of the sources of solar ultraviolet emission

Eckart Marsch
MPI für Sonnensystemforschung

Coauthors: Chuan-Yi Tu, Cheng Zhou, Li-Dong Xia, Liang Zhao, Jing-Xiu Wang, and Klaus Wilhelm

Chromospheric and Coronal Magnetic Fields,
International Scientific Conference, Lindau, Germany,
30 August – 2 September 2005

Correlating the magnetic field with VUV emission

Goal:

Search for the possible relationships between plasma flow (nascent solar wind), the VUV radiation pattern and the topology of the coronal magnetic field.

Method:

Direct comparison of the deduced velocity fields (Doppler shifts from SUMER) and line radiances with the extrapolated photospheric magnetic field for various coronal structures.

Magnetic coupling: Results from recent analyses of SUMER and MDI data, exploiting field extrapolations

Polar coronal hole

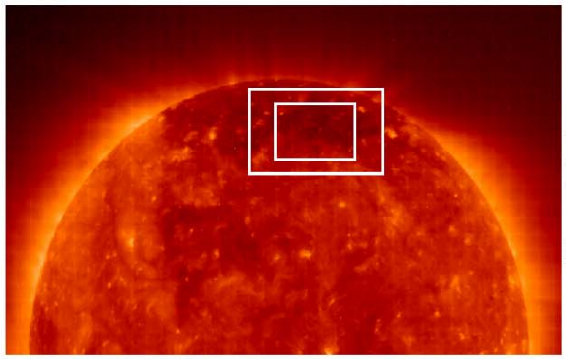

A EIT 19.5 nm

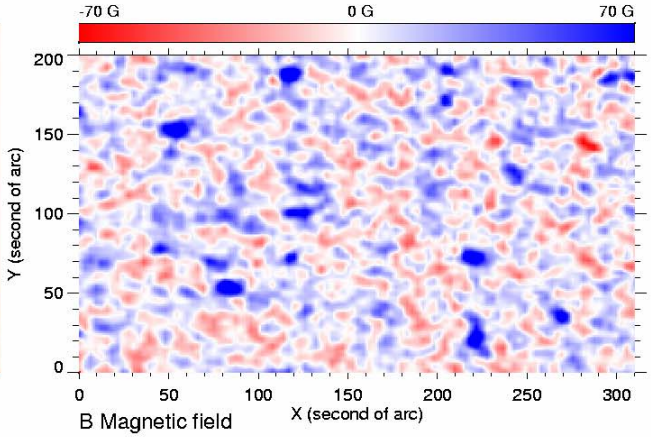

B Magnetic field

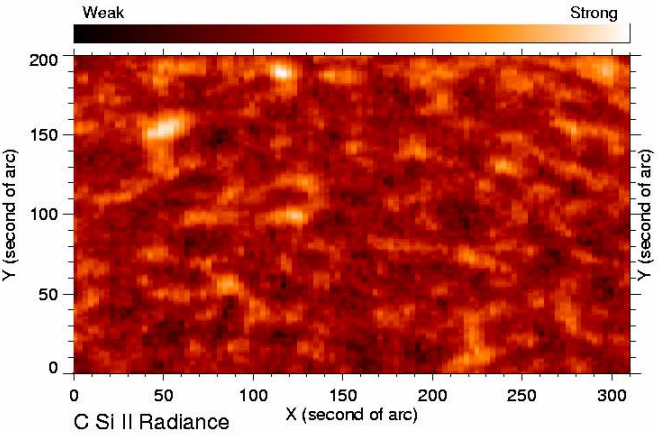

C Si II Radiance

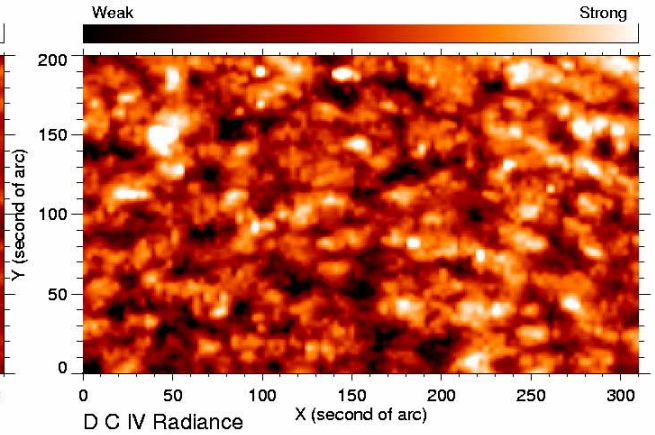

D C IV Radiance

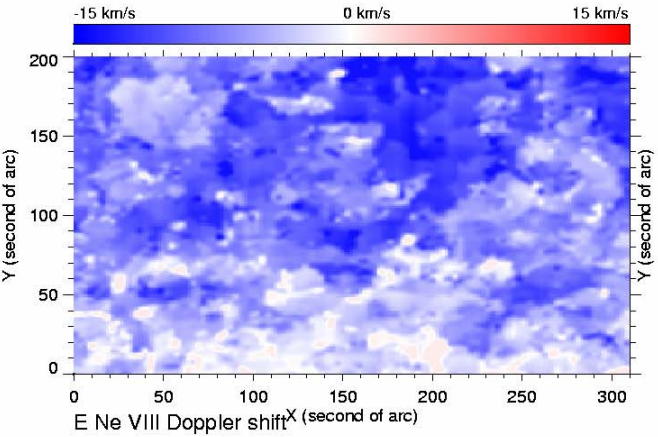

E Ne VIII Doppler shift

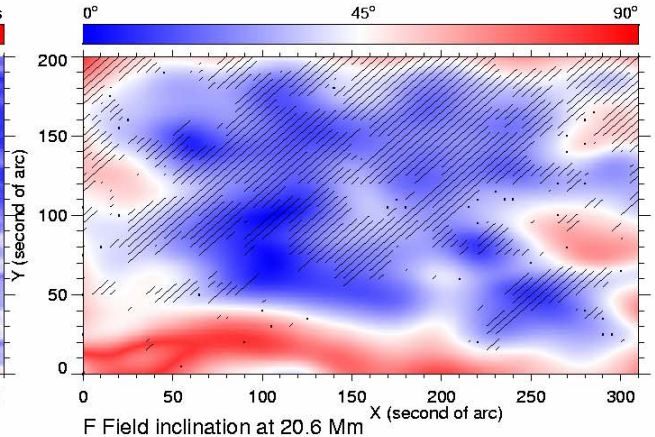

F Field inclination at 20.6 Mm

Overview

(A) Sun in EIT wavelength window around 19.5 nm. The white rectangle indicates the size of the SUMER raster scan. A comparison of the structures was made only for the smaller rectangle.
(B) Magnetic field vertical component from –70 to 70 G
(C) Si II radiance in arbitrary units (chromosphere)
(D) C IV radiance in arbitrary units (transition region)
(E) Ne VIII Doppler shifts along the LOS, ranging from –15 km/s to 15 km/s.
(F) Comparison between the Ne VIII Doppler shift (hatched regions with outflow speeds higher than 7 km/s) and the magnetic field angle, with 0° indicating vertical and 90° horizontal orientation at a height of 20.6 Mm.

Force-free magnetic field extrapolation

$$B_x = \sum_{m,n=1}^{\infty} \frac{C_{mn}}{\lambda_{mn}} \exp\left(-r_{mn} z\right) \cdot \left[\alpha \frac{\pi n}{L_y} \sin\left(\frac{\pi m x}{L_x}\right) \cos\left(\frac{\pi n y}{L_y}\right) - r_{mn} \frac{\pi m}{L_x} \cos\left(\frac{\pi m x}{L_x}\right) \sin\left(\frac{\pi n y}{L_y}\right)\right] \quad (1)$$

$$B_y = -\sum_{m,n=1}^{\infty} \frac{C_{mn}}{\lambda_{mn}} \exp\left(-r_{mn} z\right) \cdot \left[\alpha \frac{\pi m}{L_x} \cos\left(\frac{\pi m x}{L_x}\right) \sin\left(\frac{\pi n y}{L_y}\right) + r_{mn} \frac{\pi n}{L_y} \sin\left(\frac{\pi m x}{L_x}\right) \cos\left(\frac{\pi n y}{L_y}\right)\right] \quad (2)$$

$$B_z = \sum_{m,n=1}^{\infty} C_{mn} \exp\left(-r_{mn} z\right) \cdot \sin\left(\frac{\pi m x}{L_x}\right) \sin\left(\frac{\pi n y}{L_y}\right) \quad (3)$$

$$\boldsymbol{j} = \alpha \boldsymbol{B}$$

Seehafer, Solar Physics **58**, 215, 1978

definitions

$$r_{mn} = \sqrt{\lambda_{mn} - \alpha^2}$$

$$\lambda_{mn} = \pi^2 (m^2/L_x^2 + n^2/L_y^2)$$

$$2/L^2 = (1/L_x^2 + 1/L_y^2)$$

symmetry

$$B_z(-x, y) = -B_z(x, y)$$

$$B_z(x, -y) = -B_z(x, y)$$

Detailed source region

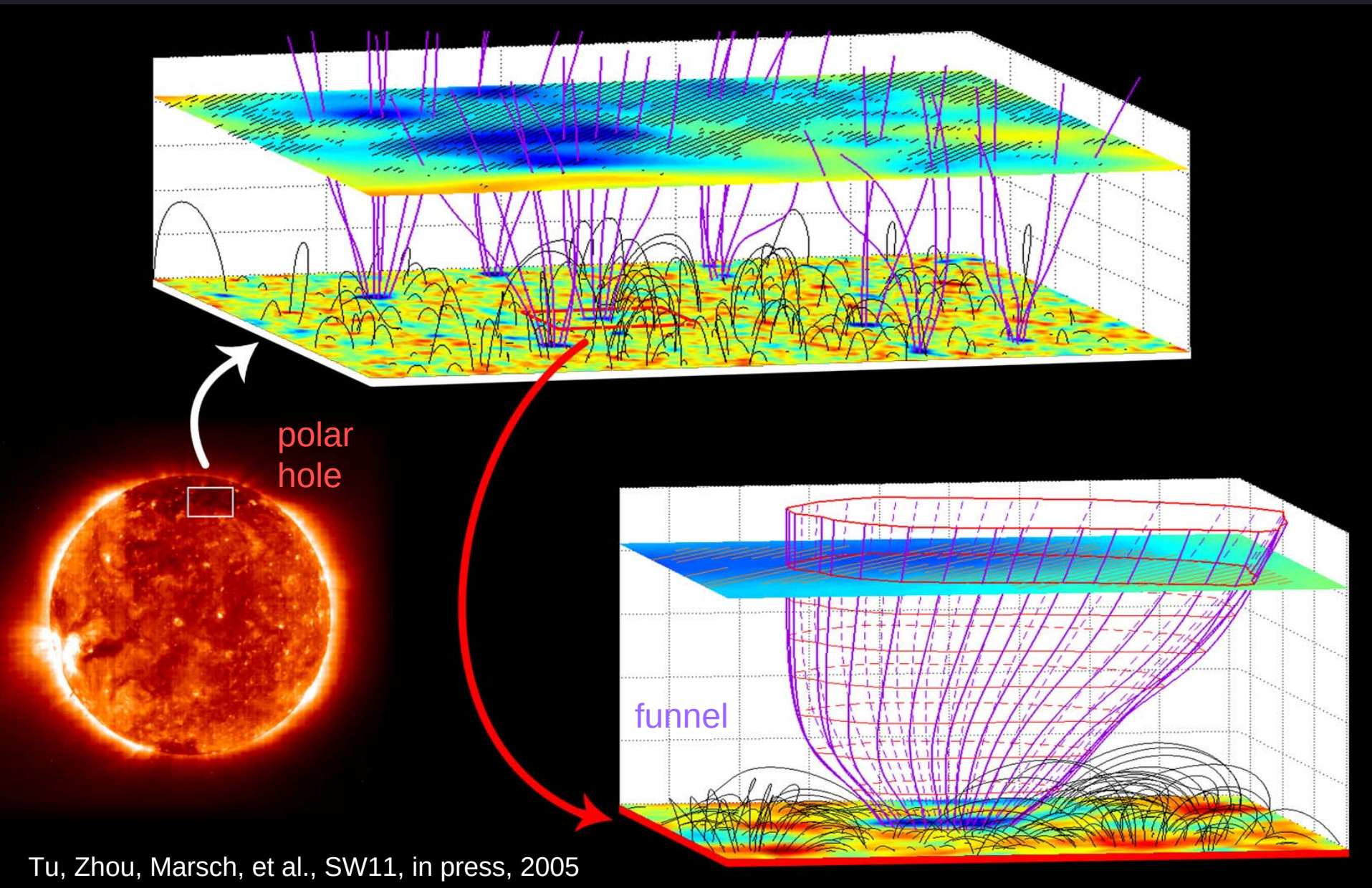

Tu, Zhou, Marsch, et al., SW11, in press, 2005

Correlating field with radiation

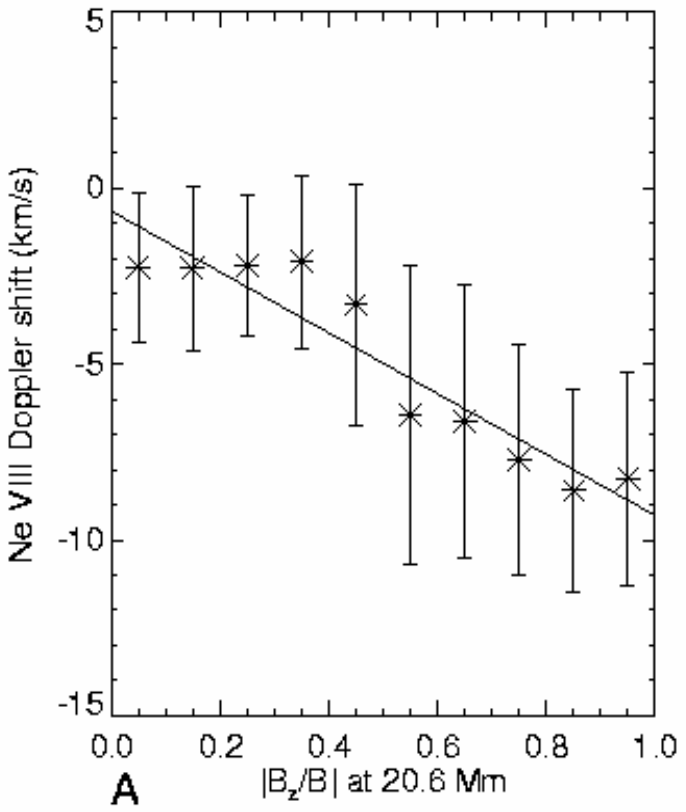

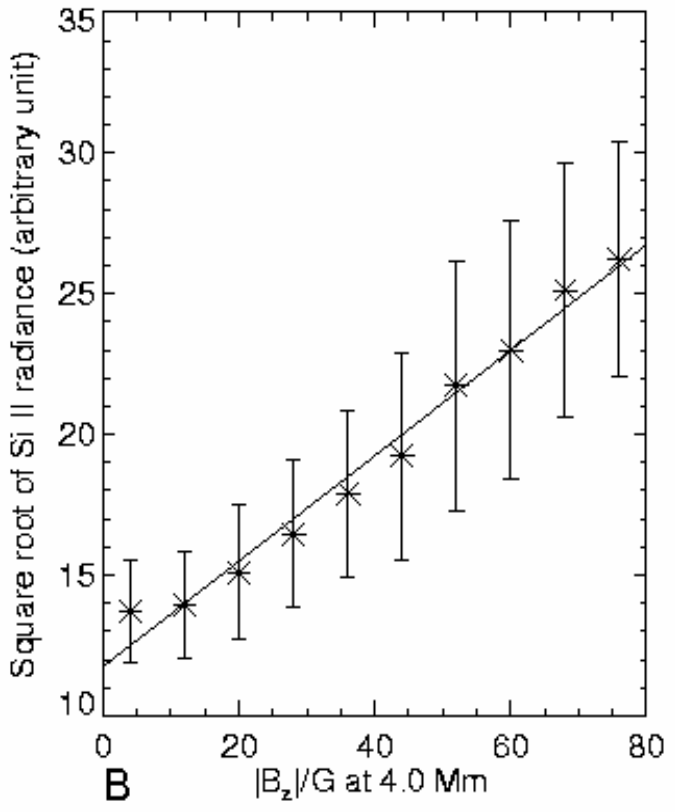

Results from the linear correlation analyses. The asterisks indicate the average values in each vertical bin, with one standard deviation. (A) Plot of the Ne VIII Doppler shift versus $|B_z/B|$ at 20.6 Mm. (B) Plot of the square root of the Si II radiance versus $|B_z|$ at 4.0 Mm.

Height variation of correlation

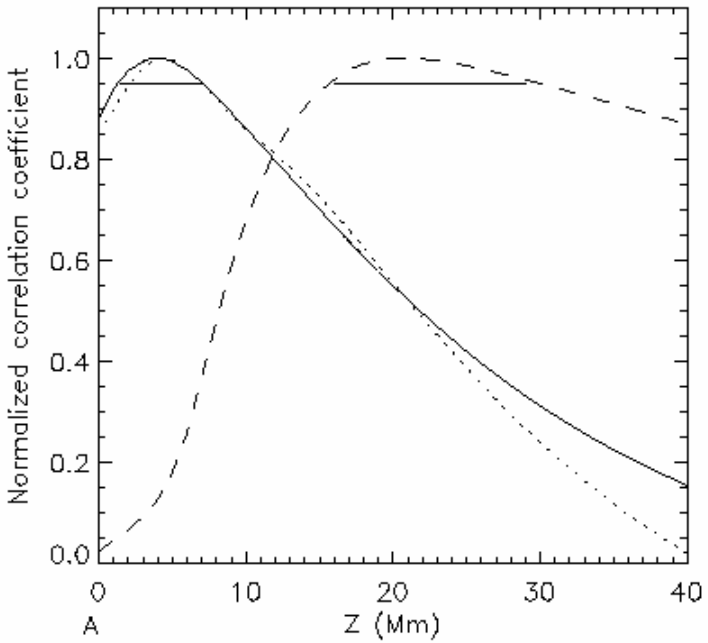

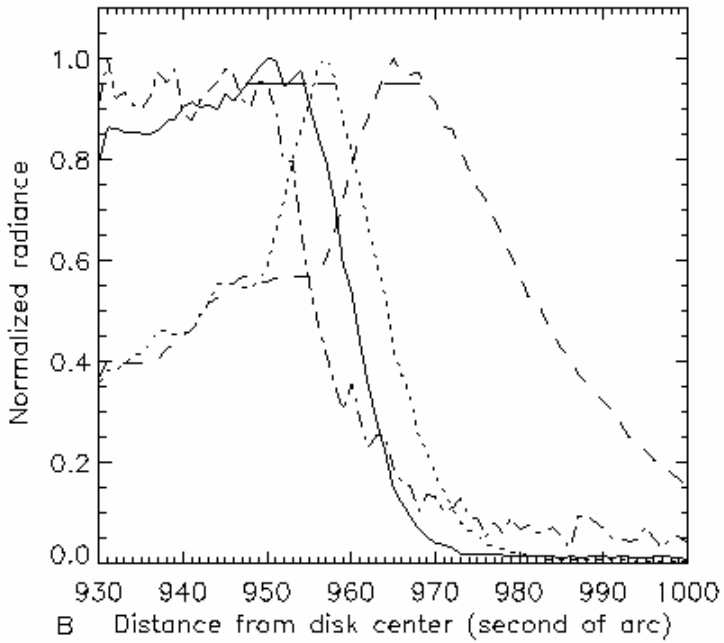

(A) The solid line gives the coefficient (normalized by 0.50) between line radiance and B_z for Si II, the dotted line the coefficient (normalized by 0.18) for C IV. The dashed line gives the coefficient (normalized by 0.39) between the Ne VIII blueshift and $|B_z/B|$.

(B) Radial variations of the line radiances of Si II, C IV and Ne VIII, and of the continuum at 154.31 nm, which is indicated by the dash-dot line. The solid line indicates Si II, the dotted C IV, and the dashed Ne VIII. All radiances are normalized to their maximum values. The data were taken across the limb.

To indicate the precision by which one can determine the maximum height, we have drawn horizontal bars extending between the two locations where the coefficients (radiances) drop below 95% of their maxima.

Correlation height in coronal hole

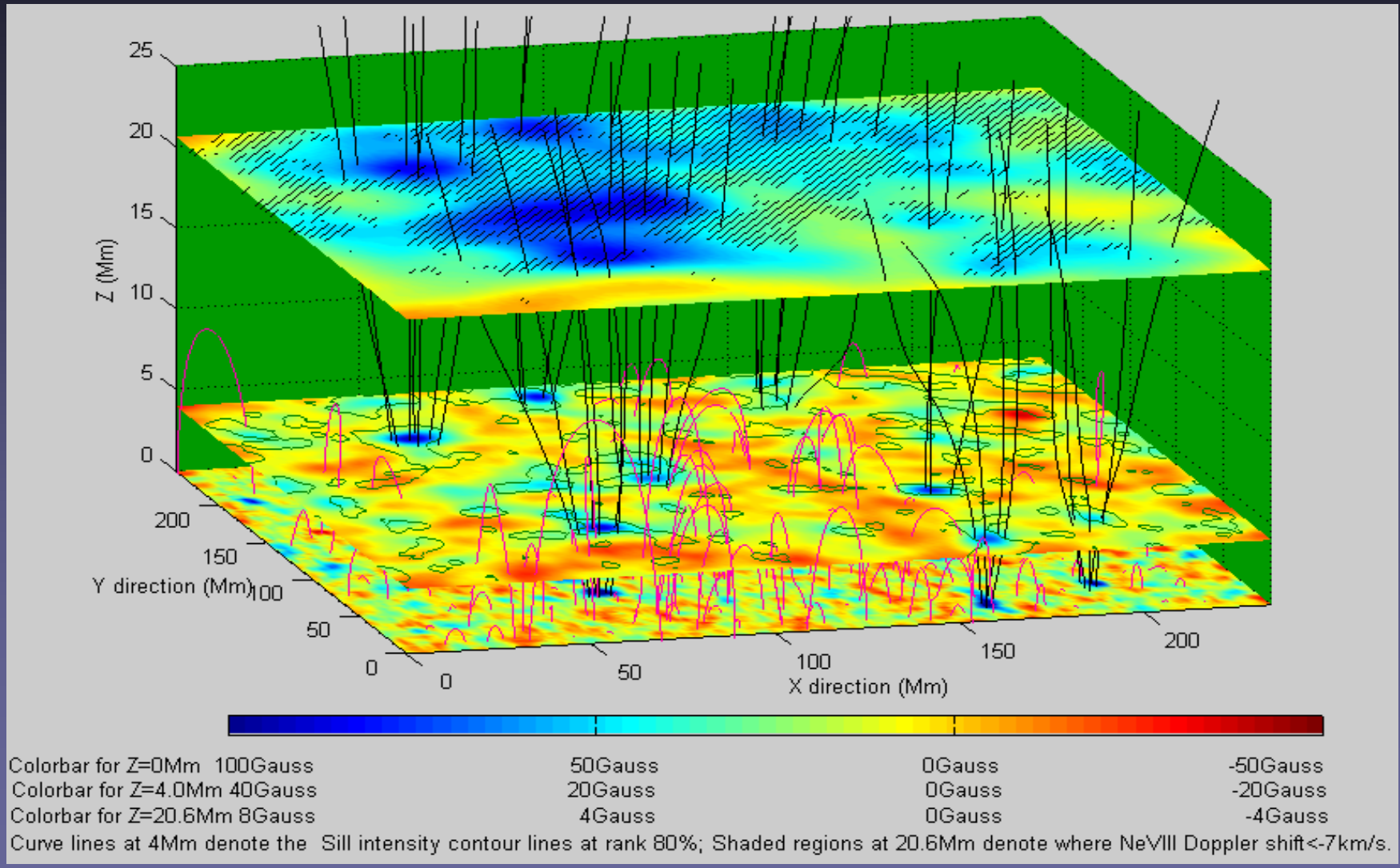

Tu, Zhou, Marsch, et al., Science, 308, 519, 2005

Correlations

field strength

field inclinaton

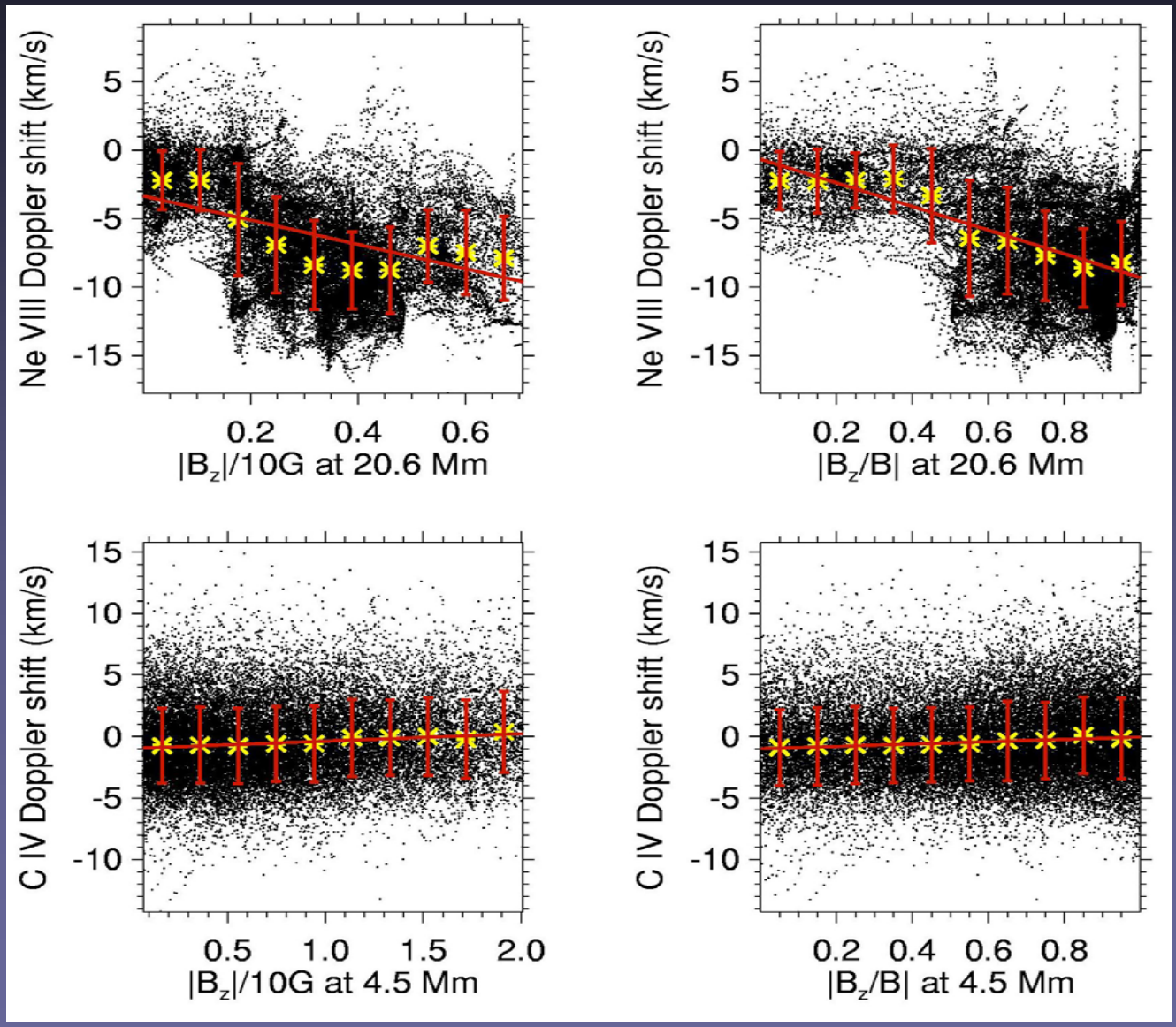

field strength

field inclinaton

Funnel geometry

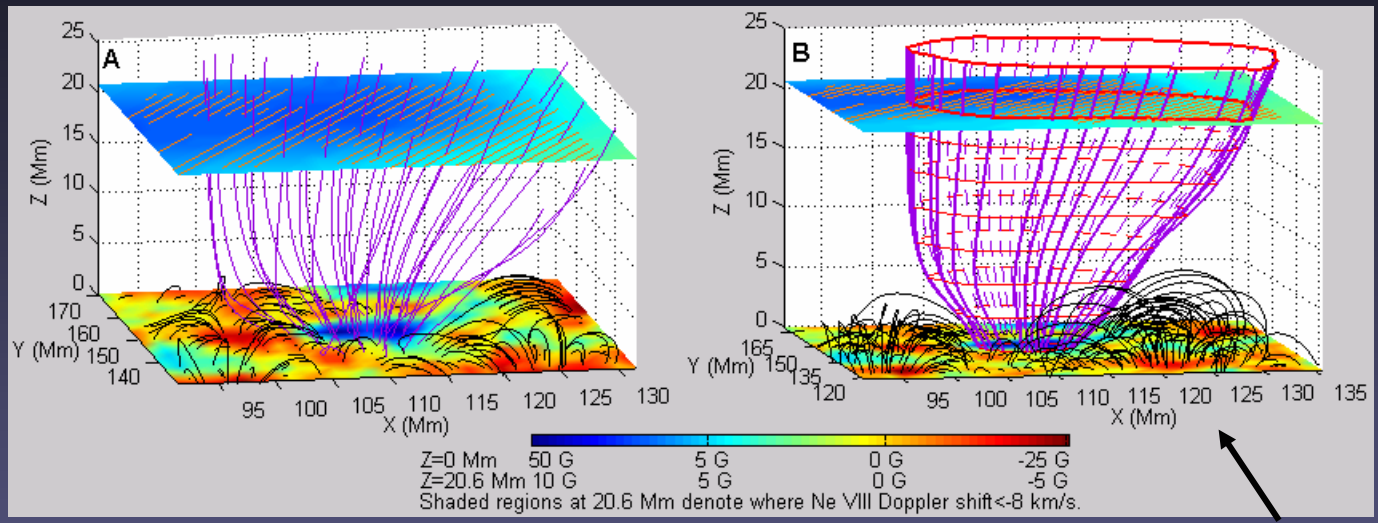

Area expands by a factor of 10

Not of canopy type!

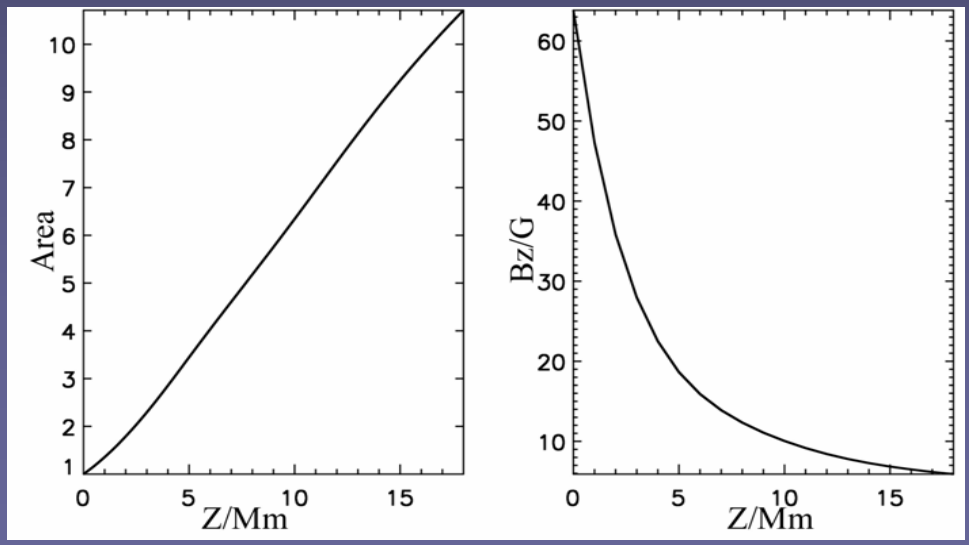

Funnel constriction by adjacent loops!

Field only declines by a factor of 6

Mass and energy supply

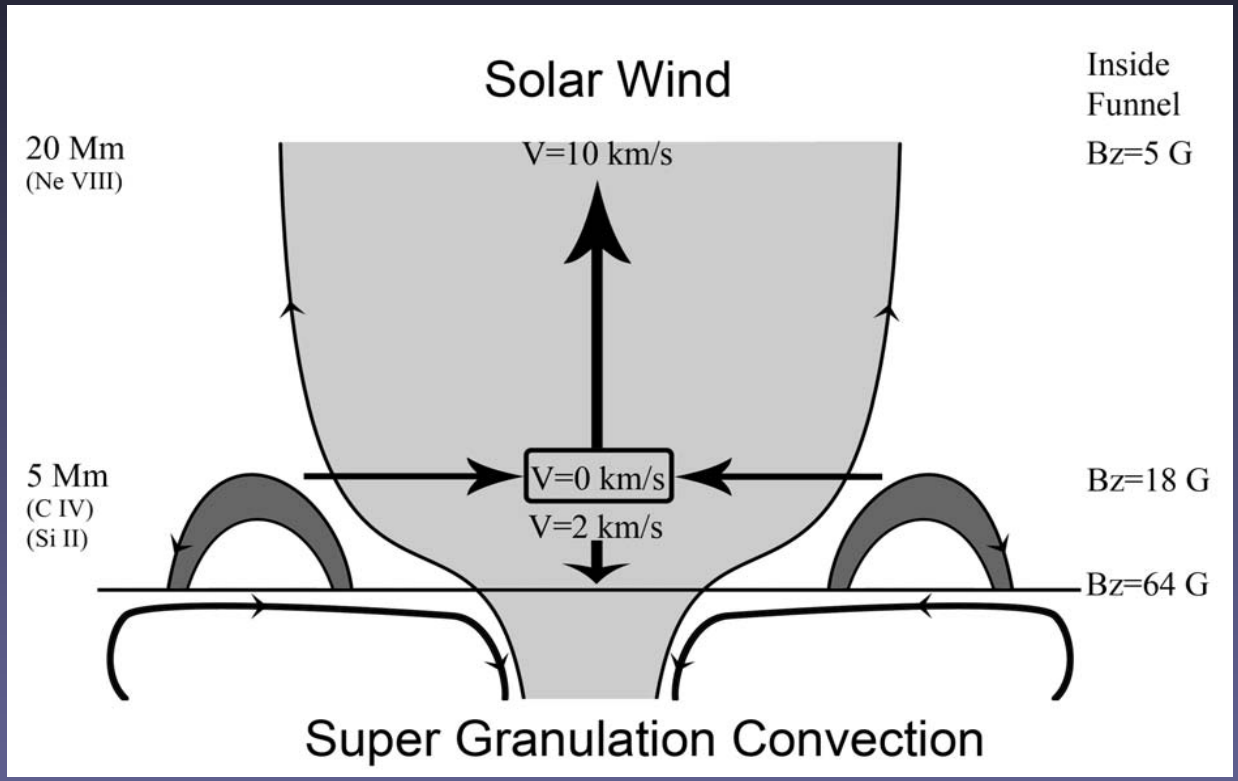

Sketch to illustrate the scenario of the solar wind origin and mass supply. The plot is drawn to show that supergranular convection is the driver of solar wind outflow in coronal funnels. The sizes and shapes of funnels and loops shown are drawn according to the real scale sizes of the magnetic structures.

Low correlation height in quiet sun

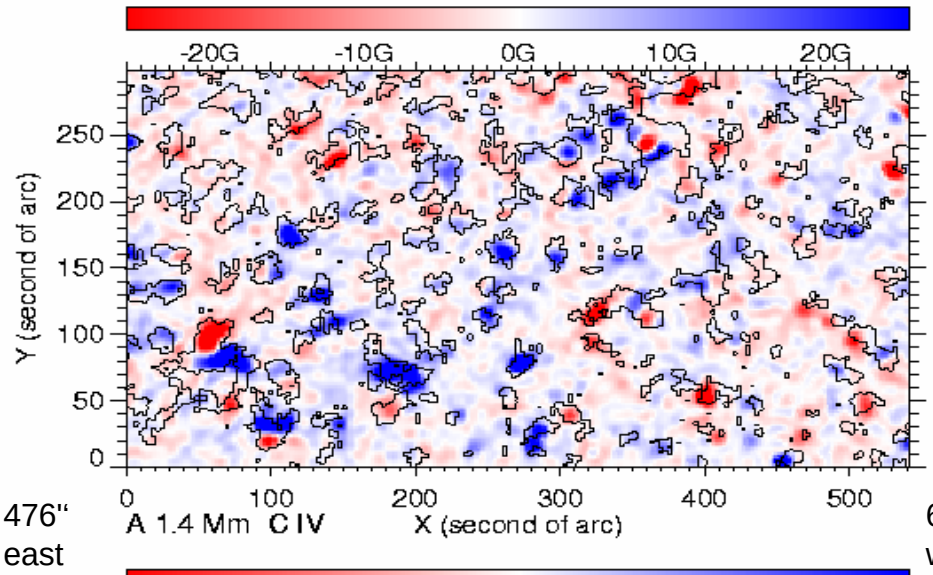

476" east

66" west

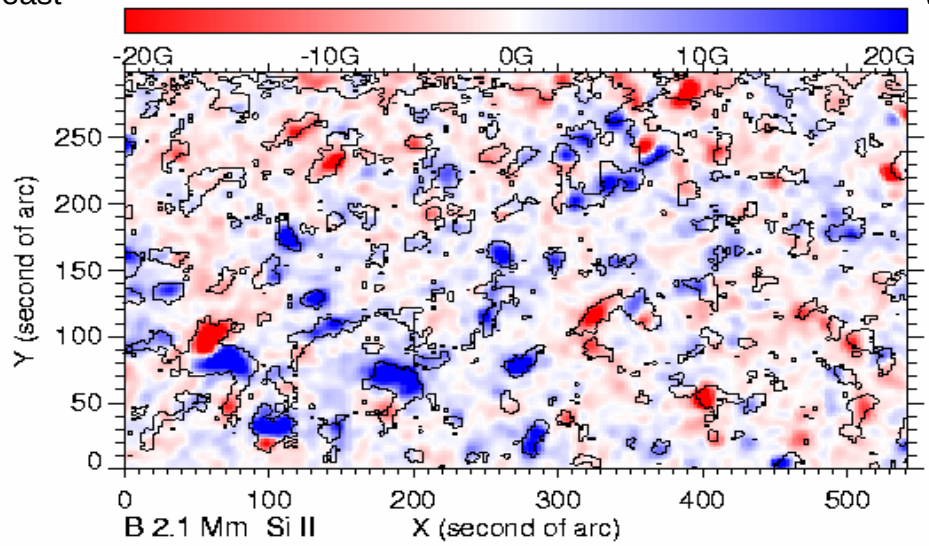

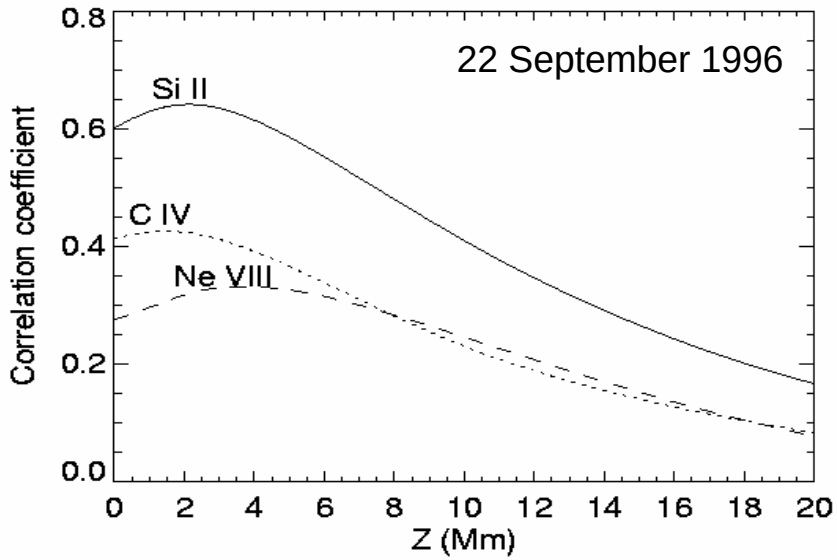

Two-dimensional maps of B_z extrapolated to 1.4 Mm (*top*) and and 2.1 Mm (*bottom*). The scale for the color coding of is given on the top of each panel. The solid lines show contours of the radiance, which ranks in the top 20% of all values in the plot, for the C IV line (*top*) and the Si II line (*bottom*). Slit center always at 411" north.

Tu, Zhou, Marsch, et al., ApJ, 624, L133, 2005

Radiance versus magnetic field

1.4 Mm

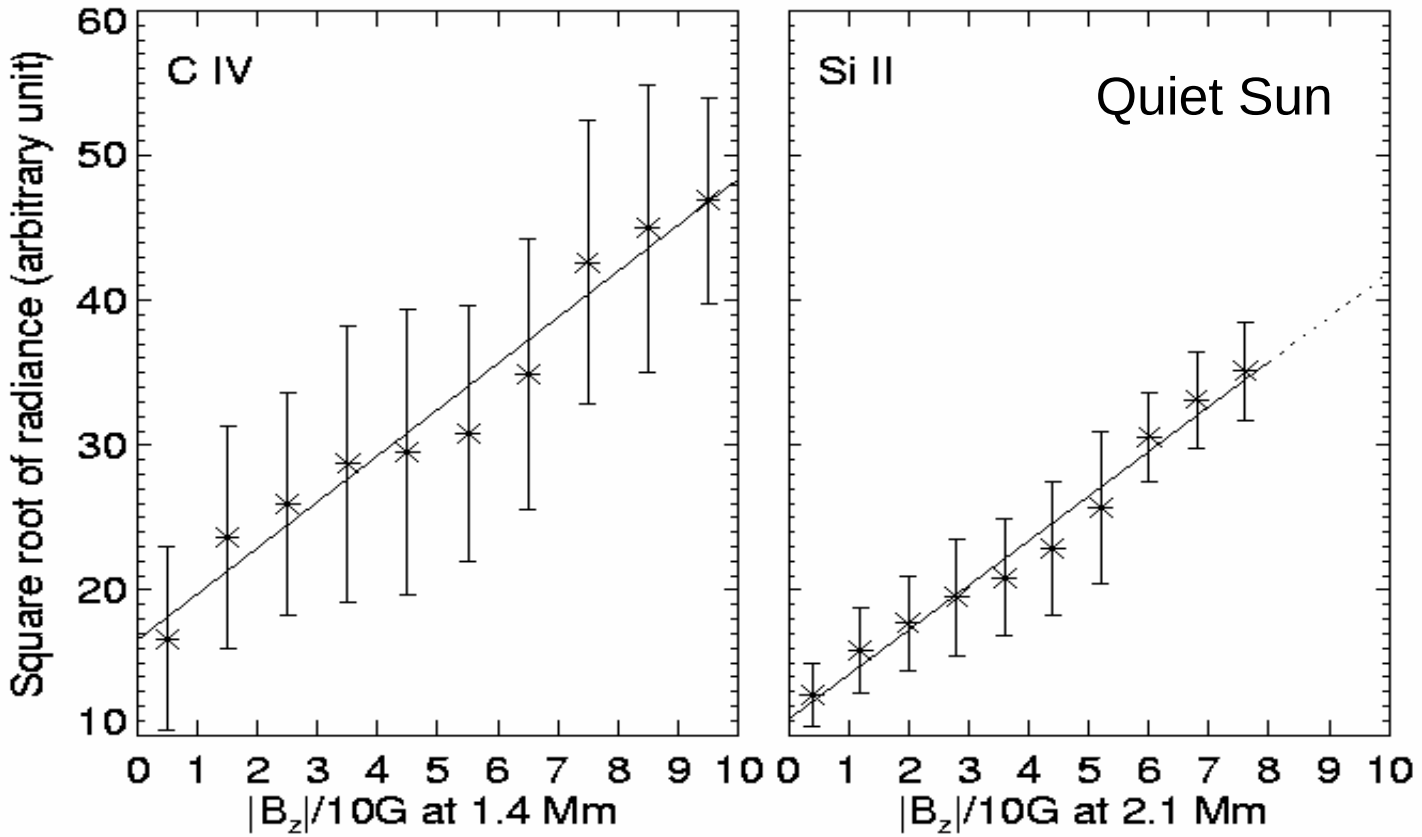

2.1 Mm

Dependence of the square root of the radiance (n_e) of the C IV (left) and Si II (right) VUV emission lines are shown (asterisks) in dependence on the vertical magnetic field strength $|B_z|$. The uncertainties are represented by the standard deviations of the averages. The solid lines give linear fits. The correlation coefficient in both cases is 0.98.

Correlation height in quiet sun

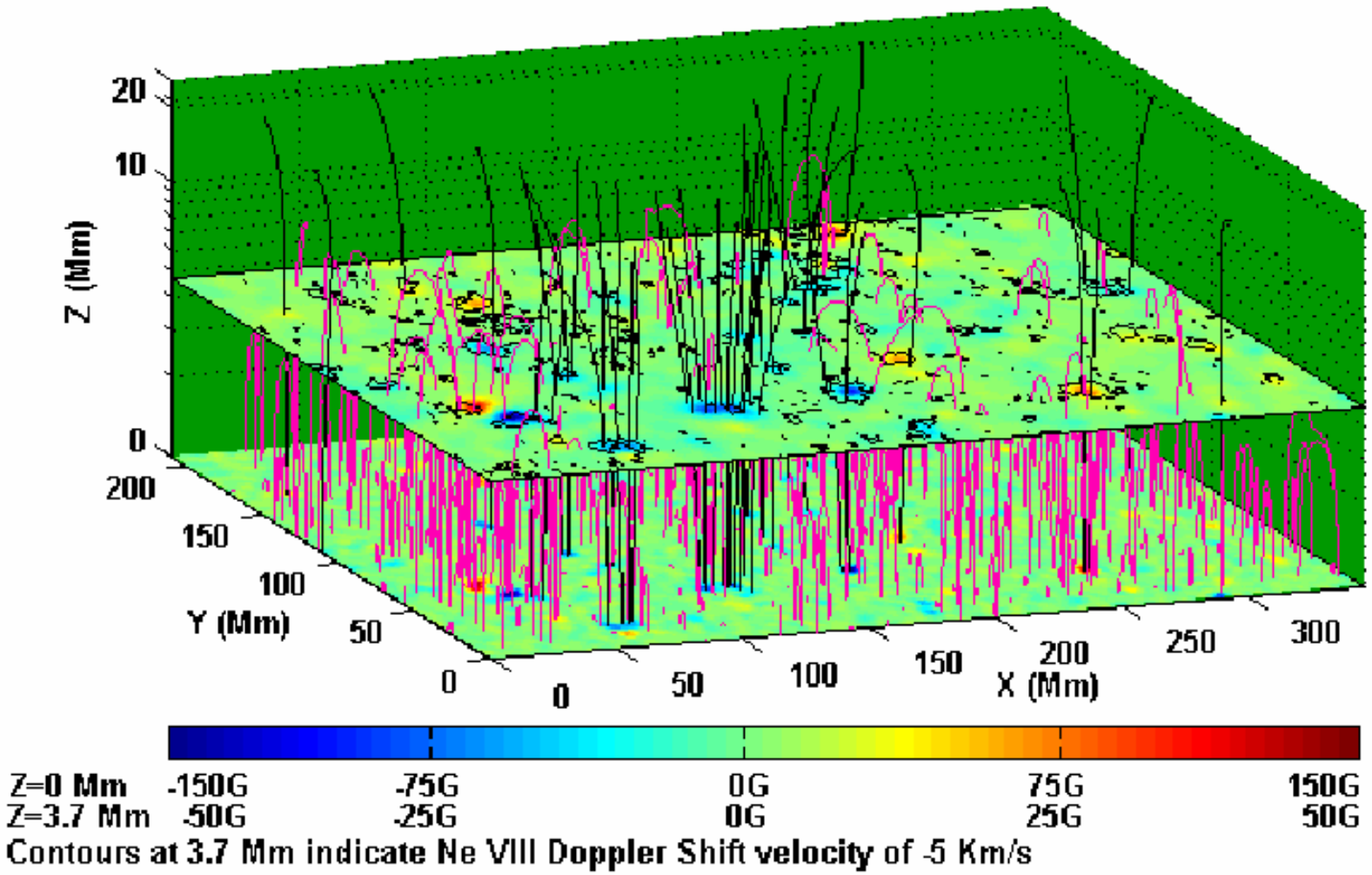

Tu, Zhou, Marsch, et al., ApJ, 624, L136, 2005

Conclusions

- Magnetic field extrapolation together with radiance and Doppler maps in various lines enables one to determine emission heights and flow geometry (in loops and funnels).
- Using (force-free) field extrapolation allows us to interpret VUV emissions in terms of field structures and to establish the dynamic magnetic couplings of atmospheric layers.